

## 5.2 CANOPY EMISSIVITY CHARACTERIZATION FROM HYPER SPECTRAL INFRARED OBSERVATIONS

Guido Masiello<sup>1\*</sup>, Giuseppe Grieco<sup>2</sup>, Carmine Serio<sup>2</sup> and Vincenzo Cuomo<sup>1</sup>

<sup>1</sup>Istituto di Metodologie per l'Analisi Ambientale del CNR, Potenza, Italy.

<sup>2</sup>Dipartimento di Ingegneria e Fisica dell'Ambiente, DIFA, Università della Basilicata, Potenza, Italy.

### 1. INTRODUCTION

Surface emissivity is one of the most critical parameters when dealing with the use and interpretation of high spectral resolution observations in the infrared. The spectral signature of the surface becomes relevant in the range with higher transmittance and, therefore, an incorrect model for the surface emissivity could sensitively bias, e.g., the retrieval of geophysical parameters in the lower part of the atmosphere.

In this work we illustrate a technique which has been used to characterize the surface emissivity of the area around our atmospheric radiation measurement (arm) site at the IMAA institute in southern Italy. The area surrounding the arm site is mostly covered by a forest. For this kind of vegetation (plant canopy), the surface emissivity is typically modeled with that of a black-body (emissivity equal to 1 and no dependence on the field of view angle). Our results show that this is, indeed, not the case and the above straightforward model can produce highly biased retrieval for temperature and water vapor.

This paper is organized as follows. Section 2 gives a brief account of the instruments involved in our study. Section 3 describes the fitting technique used for the surface emissivity. Results from this procedure are first compared to laboratory measurements and then used as input to a physical inverse scheme for the retrieval of temperature and water vapor profile. This is shown in Section 4, before the concluding remarks in Section 5.

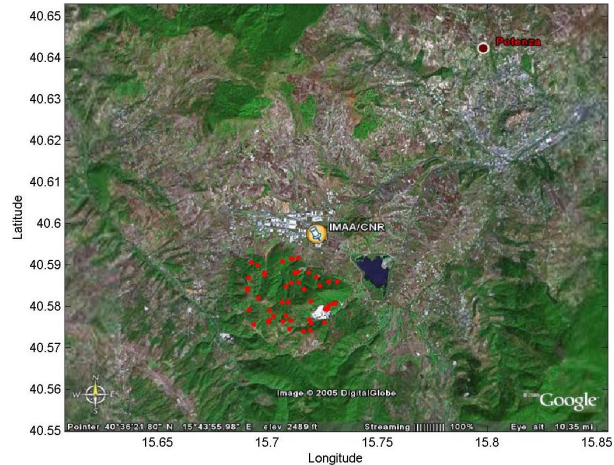


**Figure 1.** The area around the IMAA/CNR institute (the yellow mark) from Google earth (from the web site <http://earth.google.com/>). The red dots indicate the position of NAST-I footprints, whose spectra were used in our analysis.

### 2. THE INSTRUMENTS

The analysis has been performed by using NAST-I (NPOESS Aircraft Sounder Testbed Interferometer) data recorded during the Italian phase of the EAQUATE (European AQUA Thermodynamic Experiment) campaign.

NAST-I is a Fourier transform interferometer (Cousin and Gazarick, 1999) covering the spectral range between 3.7 and 15.5  $\mu\text{m}$ , with a sampling rate of 0.25  $\text{cm}^{-1}$ . It provides high spatial resolution (2.0 km footprint) atmospheric radiance from Proteus high-altitude (16 km) aircraft scanning thirteen angles of view, from  $-45^\circ$  to  $45^\circ$ , step  $7.5^\circ$ .

The international experiment EAQUATE was held in September 2004 in Italy and in the United Kingdom. One of the goals of the Italian campaign (Cuomo et al. 2005) was to demonstrate the bene-

\* Corresponding Author address: Guido Masiello, Istituto di Metodologie per l'Analisi Ambientale del CNR, IMAA/CNR, 85050 Tito Scalo, Italy; e-mail: [masiello@imaa.cnr.it](mailto:masiello@imaa.cnr.it).

	Longitude (°N)	Latitude (°E)	Time (UTC)	FOV Angle (°)	Ceilometer
1	40.59	15.70	06-Sep-04 18:01:42	15.0	Cloudy
2	40.58	15.71	06-Sep-04 18:01:56	22.5	Cloudy
3	40.58	15.73	06-Sep-04 18:02:07	15.0	Cloudy
4	40.59	15.72	06-Sep-04 18:22:18	-15.0	Cloudy
5	40.59	15.71	06-Sep-04 18:22:31	-7.5	Cloudy
6	40.59	15.71	06-Sep-04 19:19:27	7.5	Clear
7	40.58	15.72	06-Sep-04 19:19:40	7.5	Clear
8	40.57	15.72	06-Sep-04 19:39:57	-15.0	Clear
9	40.58	15.71	06-Sep-04 19:40:10	-15.0	Clear
10	40.58	15.69	06-Sep-04 19:40:22	-15.0	Clear
11	40.59	15.70	07-Sep-04 22:30:12	7.5	Clear
12	40.57	15.72	07-Sep-04 22:30:25	15.0	Clear
13	40.59	15.71	08-Sep-04 02:13:05	7.5	Clear
14	40.58	15.73	08-Sep-04 02:13:19	15.0	Clear
15	40.58	15.73	08-Sep-04 02:32:46	-15.0	Clear
16	40.58	15.71	08-Sep-04 02:32:59	-15.0	Clear
17	40.58	15.69	08-Sep-04 17:03:43	-7.5	Clear
18	40.59	15.71	08-Sep-04 17:03:55	-15.0	Clear
19	40.57	15.71	08-Sep-04 17:03:56	-7.5	Clear
20	40.58	15.70	08-Sep-04 18:12:06	-15.0	Clear
21	40.58	15.72	08-Sep-04 18:12:17	-22.5	Clear
22	40.59	15.71	08-Sep-04 19:17:49	-22.5	Clear
23	40.58	15.73	08-Sep-04 19:18:01	-22.5	Clear
24	40.58	15.69	08-Sep-04 20:23:44	-15.0	Clear
25	40.59	15.71	08-Sep-04 20:23:57	-15.0	Clear
26	40.59	15.73	08-Sep-04 20:24:09	-15.0	Clear
27	40.58	15.69	09-Sep-04 22:25:54	15.0	Clear
28	40.59	15.71	09-Sep-04 22:26:06	7.5	Clear
29	40.58	15.73	09-Sep-04 22:26:18	7.5	Clear
30	40.58	15.73	10-Sep-04 00:37:31	-7.5	Clear
31	40.58	15.71	10-Sep-04 00:37:43	-7.5	Clear
32	40.59	15.69	10-Sep-04 00:37:57	0.0	Clear
33	40.58	15.70	10-Sep-04 01:30:08	15.0	Clear
34	40.59	15.72	10-Sep-04 01:30:20	7.5	Clear
35	40.58	15.73	10-Sep-04 02:29:56	-7.5	Clear
36	40.59	15.71	10-Sep-04 02:30:08	-7.5	Clear
37	40.59	15.69	10-Sep-04 03:18:50	7.5	Clear
38	40.58	15.71	10-Sep-04 03:19:03	7.5	Clear
39	40.58	15.72	10-Sep-04 03:23:11	22.5	Clear
40	40.58	15.70	10-Sep-04 03:23:23	22.5	Clear

**Table 1.** The table summarizes basic information of the NAST-I observations used in the current analysis. Second to fifth columns show, Observed Longitude, Observed Latitude (surface-projected), acquisition time and Field of view (0 means nadir view), respectively. The last column indicates the cloud classification of the spectrum according to Ceilometer observations.

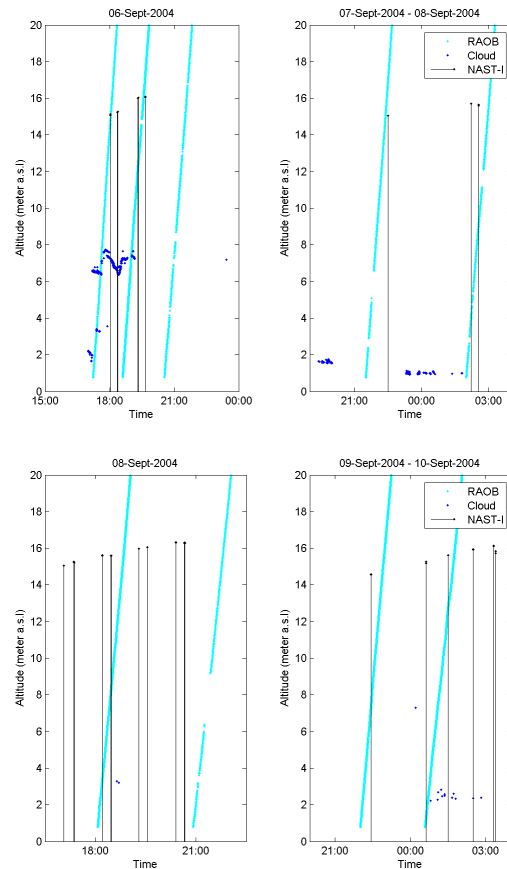


**Figure 2.** In this figure the radiosonde trajectories (in cyan) are plotted against the time. The blue dots indicate the position of the clouds detected by ceilometer. The black stems indicate the NAST-I overpass.

fit of ground-based and airborne systems to validate satellite observations (and related retrieval products) of hyper spectral infrared sensors, such as AIRS spectrometer aboard the AQUA satellite.

During the EAQUATE campaign, NAST-I flew over the southern part of Italy, at a cruise altitude of 15-16 km. The flights were held late in the afternoon and nighttime from 6 to 9 September 2004.

During the NAST-I overpasses, atmospheric temperature and water vapor were profiled by several Vaisala RS90 and RS92 sondes, with a time sampling rate of approximately 2 hours. Furthermore, a microwave radiometer (Radiometrics TP/WVP-3000) was operated continuously with a time sampling rate of 5 minutes. Finally, a Ceilometer (Vaisala CT25K), to detect the presence of clouds, was also used, with a time sampling rate of 20 seconds.

The set of NAST-I spectra, which have been used in the analysis (see Figures 1, 2, and Table 1), were recorded over a plant canopy (deciduous and conifer forest). Figure 1 illustrates the footprint position of the various observations.

### 3. FITTING SURFACE EMISSIVITY

Ancillary observations for temperature and water vapour, along with other observations from the arm site, allowed us to have an independent knowledge of the thermodynamic atmospheric state during the NAST-I flights.

Synthetic spectral radiance could be, therefore, computed and compared to the observations. The resulting spectral residual, at wave number of high transmittance, could be then minimized by properly adjusting the spectral emissivity.

Let  $p_g$  and  $p_a$  denote, respectively, the ground pressure and the aircraft altitude pressure, then the radiance observed by NAST-I can be modeled by:

$$R(\sigma) = \varepsilon_g(\sigma)B(T_g)\tau_0(\sigma) + \int_{p_g}^{p_a} B(T(p))\frac{\partial\tau}{\partial p}dp \quad (1)$$

where  $\sigma$  denotes the wave number,  $\varepsilon_g$  is the unknown surface emissivity to be determined,  $T_g$  and  $T(p)$  are respectively the surface temperature and temperature at the pressure  $p$ ,  $B$  is the Planck function, and  $\tau_0$  indicates the total transmittance from  $p_g$  to  $p_a$ .

Using a suitable first guess for the spectral emissivity (e.g. that of a black body), we can calculate the radiance from (1)

$$R_{cal}(\sigma) = \varepsilon_{fg}(\sigma)B(T_g)\tau_0(\sigma) + \int_{p_g}^{p_a} B(T(p))\frac{\partial\tau}{\partial p}dp \quad (2)$$

where  $\varepsilon_{fg}$  is a first guess emissivity, and compare it to that observed by NAST-I. If we assume that the difference between the two is solely due to emissivity, then we can derive an updated estimation for the emissivity according to:

$$\varepsilon_g(\sigma) = \varepsilon_{fg}(\sigma) - \frac{R_{cal}(\sigma) - R_{obs}(\sigma)}{B(T_g)\tau_0(\sigma)} \quad (3)$$

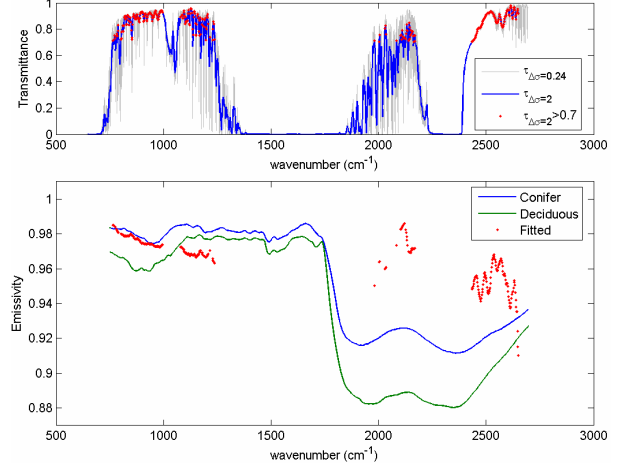


**Figure 3.** Upper panel: synthetic transmittance computed at NAST-I resolution (gray line) and resolution of  $2 \text{ cm}^{-1}$  (blue line). The red dots show the channels used for the fitting procedure of the surface emissivity. Bottom panel: fitted emissivity (red dots) compared to laboratory measurements (blue and green lines, conifer and deciduous emissivity, respectively).

This Equation must be handled with some precaution. In fact, it is easy to notice that, for small transmittance, the uncertainty on rapidly increase. Moreover the lack of information on trace gases profiles could strongly bias the surface emissivity.

For these reasons we used Equation (3) only for those wave numbers characterized by higher transmittance (the threshold  $\tau_0 > 0.7$  was used, in practice) Moreover, to filter out the possible effects due to the lack of precise information on trace gases amount (particularly  $\text{N}_2\text{O}$ ,  $\text{CH}_4$  and  $\text{CO}$ ), synthetic and observed spectral radiance were re-sampled at a rate of  $2 \text{ cm}^{-1}$ . For the same reason, we did not consider the Ozone band at  $9.6 \mu\text{m}$ .

The computation of synthetic spectral radiance was performed by using last version (v9.4) of LBLRTM (Clough and Iacono 1995), HITRAN2004 (Rothman et al. 2005) for the spectral-lines database, and the water vapour continuum model MT\_CKD1.2 (Tobin et al. 1999) were used.

The atmospheric state vector used in the calculations has been obtained by a linear time interpolation of two consecutive radiosonde profiles. The water vapour profile is then further adjusted by constraining it to the microwave water vapour columnar contents. For the trace gases concentration we use climatology. The  $\text{CO}_2$  profile was set to a constant mixing ratio equal to 373 ppmv.

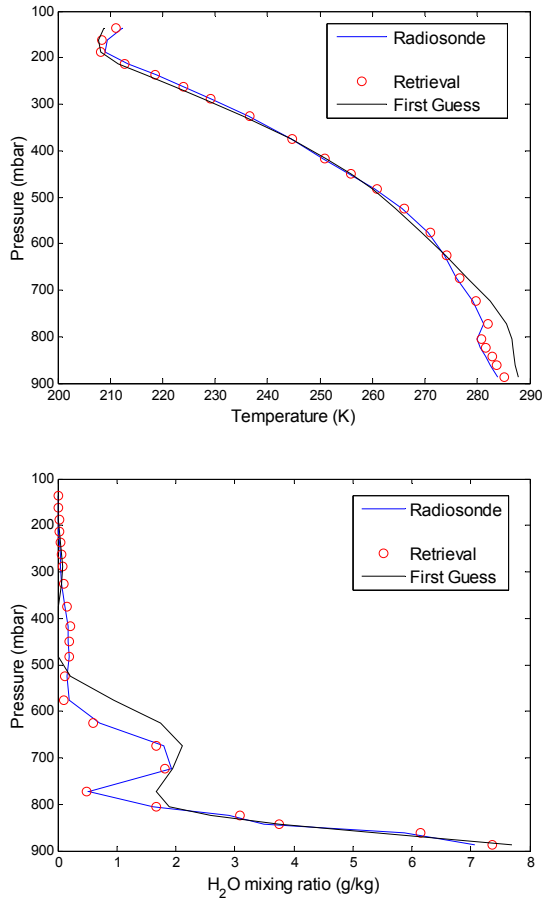


**Figure 4.** Example of NAST-I retrieval for temperature and water vapor; the NAST-I spectrum used for the inversion was recorded during the night of 9-September at 22:26:06 GMT (the spectrum number 28 in Table.1). The retrieval (open circles) is shown along with the radiosonde observation (blue line) and the First Guess (black line).

Results of the technique are shown in Figure 3, where (upper panel) we show the synthetic transmittance computed at the NAST-I resolution (gray line). This transmittance, re-sampled at resolution of  $2 \text{ cm}^{-1}$ , is shown in blue, whereas the red dots refer to the channels ( $2 \text{ cm}^{-1}$  resolution), with transmittance larger than 0.7.

The red dots in the bottom panel of Figure 3 show the fitted emissivity using the spectra listed in Table 1 with field of view equal to  $\pm 7.5^\circ$ . The resulting emissivity is compared to laboratory measurements (Salisbury and D’Aria 1992) again in Fig. 3.

It is possible to see that there is a good agreement with the Conifer emissivity (the blue line in the lower panel of Figure 3) in the long wave region, around  $11 \mu\text{m}$ , whereas a relatively

large discrepancy is seen in the shortwave region. A relevant difference appears also in the atmospheric window at  $9 \mu\text{m}$ .

#### 4. RETRIEVAL OF TEMPERATURE AND WATER VAPOR PROFILE

The emissivity, retrieved as described in Section 3, has been then used to invert NAST-I observations for temperature and water vapor retrieval. The inversion scheme we used is that implemented in the so-called  $\delta$ -IASI package (Carissimo et al. 2005). The scheme follows a data constrained optimization which generalizes the usual Statistical Regularization estimator to the class of ridge regression estimator. The forward model embedded in  $\delta$ -IASI is  $\sigma$ -IASI (Amato et al. 2002) a fast line-by-line model that, in addition to spectral radiance, computes analytical Jacobians for the major geophysical parameters (e.g. temperature, water vapour, ozone, carbon dioxide, nitrous oxide).

Figure 4 shows the inversion for temperature and water vapor for the spectrum recorded the night of 9-September at 22:26:06 GMT, with an angle-of-view of  $7.5^\circ$ . This spectrum was not included in the data set used for fitting the surface emissivity.

The inversion (red circles) shows a very nice agreement with radiosonde observations both for temperature and water vapor. At the same time, the residual between retrieved and observed spectra is smaller than 2 times the NAST-I radiometric noise (see Figure 5).

#### 5. CONCLUSION AND FUTURE WORKS

We have described a technique to characterize the surface emissivity of a green-forest area around our arm site at the IMAA institute in southern Italy. The fitted emissivity, once compared to laboratory data, showed a good agreement in the long wave region (around  $11 \mu\text{m}$ ), with Conifer emissivity, but significant differences appeared in the short wave region.

The technique provides emissivity shapes consistent with both forward and inverse calculations and, therefore, it is effective to characterize target areas to be used in remote sensing experiments from Space, e.g., validation and calibration campaigns of satellite data and products.

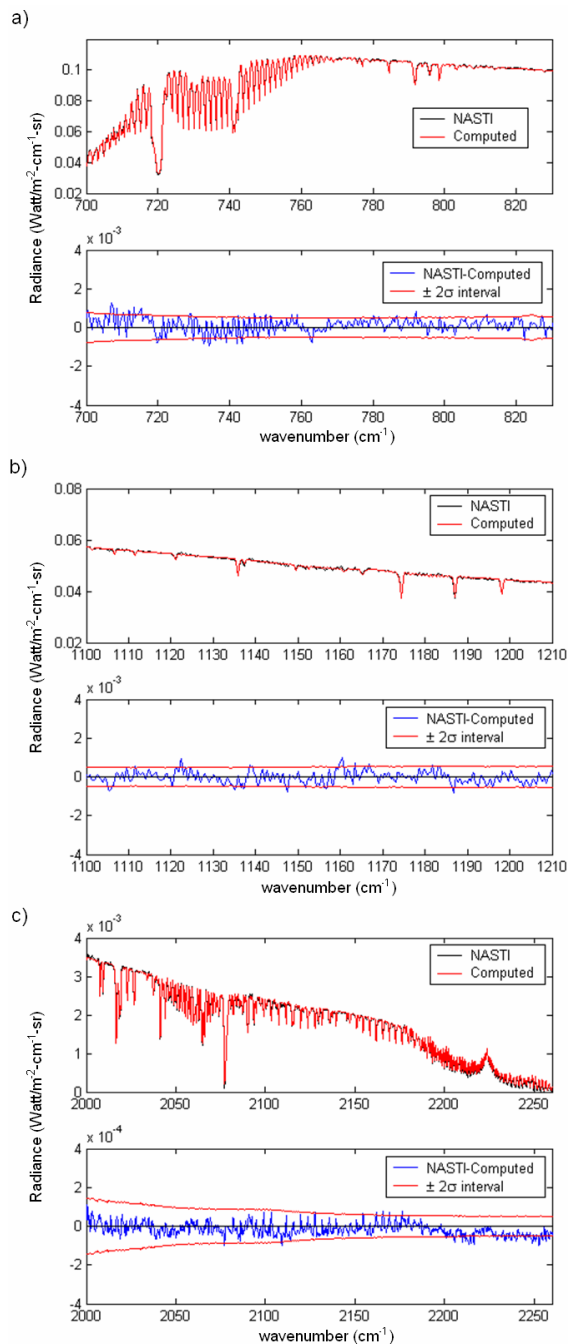


**Figure 5.** The figure shows the consistency between NAST-I (experimental) and  $\sigma$ -IASI (fitted) spectral radiance. The case shown refers to the retrieval exercise illustrated in Fig. 4. The three panels refer to the spectral ranges a)  $700\text{--}830\text{ cm}^{-1}$ , b)  $1100\text{--}1210\text{ cm}^{-1}$ , c)  $2000\text{--}2260\text{ cm}^{-1}$ . The  $\pm 2\sigma$  interval has been computed on the basis of the NAST-I radiometric noise.

The fundamental needs of this technique are easily available in any arm site and are:

- a) homogeneous footprint;

b) well co-located independent observations of the thermodynamic state of the atmosphere.

In the future we will focus our analysis on investigating possible dependence of canopy emissivity on the angle-of-view.

## REFERENCES

- Amato, U., G. Masiello, C. Serio, M. Viaggiano, 2002. The  $\sigma$ -IASI code for the calculation of infrared atmospheric radiance and its derivatives. *Environmental Modelling & Software* **17**, 651–667.
- Carissimo, A., I. De Feis, C. Serio, 2005: The physical retrieval methodology for IASI: the  $\delta$ -IASI code, *Environmental Modelling & Software*, **20-9**, 1111-1126
- Clough, S.A. and M.J. Iacono, 1995: Line-by-line calculations of atmospheric fluxes and cooling rates II: Application to carbon dioxide, ozone, methane, nitrous oxide, and the halocarbons. *J. Geophys. Res.*, **100**, 16519-16535.
- Cousins, D. and M.J. Gazarick, 1999: NAST Interferometer Design and Characterization. *Final Report, MIT Lincoln Laboratory Project Report NOAA-26, July 13, 1999.*
- Cuomo, V. et al. 2005: The Italian phase of the EAQUATE measurement campaign. *SPIE proceedings* **5979**, 396-409.
- Rothman, L.S. et al., 2005: The HITRAN 2004 molecular spectroscopic database. *Journal of Quantitative Spectroscopy & Radiative Transfer* **96**, 139–204.
- Salisbury, J. W. and D.M. D’Aria, 1992: Emissivity of terrestrial materials in the 8-14  $\mu\text{m}$  atmospheric window, *Remote Sensing of the Environment*, **42**, 83-106.
- Tobin, D.C. et al., 1999: Down-welling Spectral Radiance Observations at the SHEBA Ice Station: Water Vapor Continuum Measurements from 17-26 micrometer. *J. Geophys. Res.*, **104**, 2081-2092.